ISSN: 2710-0588

Numerical Simulation of Mechanical Properties of Deep Gray Sandstone with Holes and Radial Cracks

Lele Yuan[1, a]

[1]School of Civil Engineering, Henan Polytechnic University, Jiaozuo, China

[a]17639403483@163.com

Abstract

In order to study the effects of prefabricated pore-fracture on the mechanical properties, crack extension and energy evolution of rocks under uniaxial compression, the effects of rock samples containing pore-fracture deep grey sandstone on the mechanical properties, crack extension and energy evolution of rocks were analysed in detail through the indoor experimental inverse performance of the fine-scale mechanical parameters of the PFC3D model. The results show that the mechanical parameters of deep grey sandstone samples with pore fissures are significantly lower than those of intact samples, and the decrease is closely related to the diameter of the pore as well as the length and width of the fissure, with the increase of the diameter of the pore, the peak strength and the peak strain of deep grey sandstone with single pore are in the trend of attenuation, and the mechanical parameters of deep grey sandstone samples with pore fissures of different lengths and widths are in the trend of attenuation with the increase of fissure widths and lengths of different layers. The mechanical parameters of deep grey sandstone samples with different lengths and widths of fissures show a trend of attenuation with the increase of fissure width and length; based on the analysis of microscopic crack characteristics during loading of deep grey sandstone with pore fissures, it is concluded that the cracks produced by deep grey sandstone samples with pore fissures are mainly distributed at the two ends of the samples, and the middle area has fewer cracks and the number of the cracks produced shows a trend of attenuation with the increase in the diameter of the pore as well as the length and width of the fissure; Based on the energy evolution mechanism, it is concluded that as the pore size of the rock sample increases, the strain node at which the dissipated energy begins to appear becomes progressively earlier, the energy storage capacity of the rock appears to be drastically reduced, and the internal damage becomes more and more severe.

Keywords

Dark grey sandstone; Pore fissures; Microscopic cracks; Energy evolution.

1. Introduction

Rocks are not only widely distributed in complex natural tectonic bodies, but are also important materials widely used in engineering. And the rock body usually has defects such as holes and fissures of different shapes and sizes, which can complicate the structural and mechanical properties of the rock body and may lead to damage and instability. In engineering practice, various types of defects and their forms of distribution in the rock have a significant influence on the mechanical properties of the rock and the damage process. Therefore, carrying out the research on the mechanical mechanism and crack extension characteristics of rocks under the action of defects has an important application value in many rock engineering. At present, many researchers at home and abroad have done a lot of research on defect-containing rocks.

ISSN: 2710-0588

Li Diyuan et al [1] investigated the changing law of dynamic compressive mechanical properties such as dynamic mechanical parameters, crack extension evolution process and final damage mode of laminated rocks with prefabricated centre holes under different laminar inclination conditions; Yang Shengqi et al[2] conducted a series of uniaxial compression experiments on pore-bearing fissured sandstone. On this basis, the strength and deformation properties of the pore-bearing fissured sandstone specimens were analysed; Li Xuehua et al [3] used indoor uniaxial compression experiments and PFC2D model experiments to comparatively study the elastic modulus, peak strength and other related indexes of intact sandstone and single-fractured sandstone specimens, as well as comparative studies with the final damage patterns of the specimens; Fu Mingzhi et al [4] analysed the compressive strength, elastic modulus, damage patterns, and crack expansion of rocks with different pore-fracture combinations distributions through uniaxial compression tests; Duan Jinchao et al [5] carried out a simulation study on the damage of brittle rocks containing holes under uniaxial compression conditions, and the results of the study showed that the presence of holes has a great influence on the mechanical properties and damage modes of rocks; Han Guansheng et al [6] carried out a series of uniaxial compression tests of circularly porous sandstones with different pore diameters and shape arrangements to obtain the strength, deformation and damage process. The interaction mechanism between the rock pores and the influence of the pores on the mechanical behaviour of the rock were investigated; Qingwen Zhang et al [7] studied the influence of the inclination angle of the two pores on the peak strength, peak deformation and crack development based on indoor uniaxial compression tests of sandstone by using particle flow numerical simulation software through unidirectional compression experiments with two pores at different angles; Zhu Tan Tan et al [8] conducted indoor uniaxial compression tests on plate-like sandstone specimens with different pore centre spacing and different inclination angles of double circular holes, and concluded that the pore centre spacing and inclination angle have a large influence on the strength and deformation characteristics of sandstone, as well as on the damage evolution process; Xie Maolin et al [9] conducted numerical simulation tests of the whole process of damage of pore-bearing rock specimens under the uniaxial, biaxial, and triaxial loading conditions by using the RFPA3D-Parallel program based on the massively parallel computing environment of Northeastern University, respectively. The numerical simulation test of the whole process when the rock sample is under uniaxial and triaxial loading conditions; Zhang et al [10] investigated the crack extension and penetration characteristics of single fissure at different angles through numerical simulation; Gong Shuang et al [11] carried out the experimental study on the damage characteristics of limestone specimens with double pore fissures under impact conditions, and the results show that the shape, spacing and asymmetry of limestone specimens with double pore defects will have an important influence; Wang et al [12] conducted uniaxial compression tests on specimens with different pore diameters, and concluded that the elastic and dissipation energies of specimens with different pore diameters changed with the compression process, and the energy distribution inside the specimens also changed; Li Yuanhai et al [13] conducted uniaxial and biaxial loading tests on soft rock with four cracks of different inclination angles uniformly distributed around the central hole using FLAC 3D numerical simulation software, and investigated the mechanical properties and damage forms under these conditions; Huang Shuling et al [14], in order to study the characteristic strengths of the rock body, based on the transverse isotropy theory, proposed the transverse isotropic crack strain method adapted to the rock body to solve the characteristic strengths of each feature; Fan et al [15], under uniaxial compression, gave the stress distribution around the cracks and holes under different loading stages and different defect directions, and analysed the crack and hole surrounding principal stress evolution law; Li et al [16] used prefabricated rock-like specimens with different types of defects, and then conducted uniaxial compression tests on the specimens, and compared and analysed the experimental results with the

ISSN: 2710-0588

simulation results, to obtain the order of crack initiation, crack extension phenomenon and the overall damage mode of the rock in rock specimens with different types of defects; Du, Mingrui, et al [17] obtained the crack initiation sequence, crack expansion phenomenon and overall damage mode of the rock in rock specimens with different defects by prefabricating an ellipse-shaped hole inside the plate-like rock, and using the DDL500 rock mechanics servo test system for uniaxial compression test, derived the elliptical hole biaxial load between the different angle on the strength of the rock specimen, deformation and damage characteristics of the influence of the law; Zhang Barge et al. [18] uniaxial compression test of marble containing different number of holes and different pore sizes, and before and after the destruction of the morphology of the rock samples, respectively, CT scanning, to study the damage cracks germination, expansion and the final destruction of spatial distribution characteristics. The spatial distribution characteristics of the damage cracks at the final destruction were investigated. From the experimental results, it is concluded that the number of holes and different pore diameters have a greater influence on the strength, deformation, damage form and damage degree of the specimen; Wang Yunfei et al.[19][20] carried out the mechanical tests of the rock body under different stress conditions, to reveal the energy evolution mechanism of the rock rupture under various peripheral conditions, to reveal the acoustic emission and the evolution of the strain energy of the rock rupture, and to establish a mechanical model; Cheng Hongming et al.[21] carried out the uniaxial compression tests of marble and CT scanning of the rock samples before and after damage to study the spatial distribution characteristics of the damage crack germination, expansion and final damage. et al [21] explored the correspondence between the energy transformation and the progressive damage process of specimens and the influence of fissure inclination angle on the energy transformation. Yu Yang et al. [22] used uniaxial compression, acoustic emission monitoring and X-ray diffraction test to analyse the mechanical properties of granite with different corrosion time, and obtained the change rule of acoustic emission parameters.

This shows that the study of defect-bearing rocks is very important. For this reason, in this paper, the particle flow numerical simulation software PFC is used to construct a rock sample model of dark grey sandstone containing pores and pore fissures, and to study its effect on strength, deformation, number of microcracks, expansion mode and energy evolution mechanism under uniaxial compression test.

2. Basic Parameters and Numerical Modelling

2.1. Overview of the particle discrete element procedure

In this paper, PFC3D is used to investigate the mechanical properties of prefabricated porous and fissured rocks and some laws. The input computational parameters for numerical simulation using PFC are fine-grained parameters, which mainly contain two key parameters, namely, the physical geometry parameters and the contact intrinsic parameters. Since the object of simulation is rock, the newly added Flat- jointed model (FJM) can more realistically respond to the mechanical properties of the rock material than the parallel bonded model, and it has been built into the latest version 5.0 of the PFC software, so it can be used directly, so the Flat- Jointed model is chosen as the contact model.

2.2. Parameterisation and modelling

Firstly, the stress-strain curves of the intact dark grey sandstone were obtained from the uniaxial compression test conducted indoors, from which the fine mechanical parameters of the model were inverted. Fig. 1 shows the experimental system and the uniaxial compression damage characteristics of the dark grey sandstone, and Fig. 2 shows the comparison of the

ISSN: 2710-0588

stress-strain curves of numerical simulation tests and indoor tests by adjusting the parameters, and the fine parameters obtained are shown in Table 1.


(a) experimental system


(b) Dark grey sandstone damage specimen

Figure 1. Mechanical experiment of deep grey sandstone

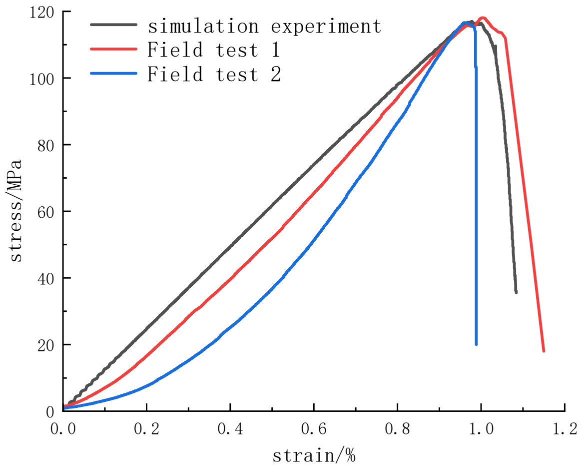

Figure 2. Comparison of stress-strain curves of sandstone

Table 1. Mesoscopic mechanical parameters of deep grey sandstone

parametric	value	parametric	value
Model height H/mm	100	Flat Nodal Stiffness Ratio kn/ks	1.0
Model Diameter W/mm	50	Flat knuckle tensile strength σb/MPa	12
Particle friction factor μ	0.5	Flat and straight nodal cohesion Cb/MPa	51
Minimum particle radius Rmin/mm	0.15	Angle of internal friction of flat joints φb /(°)	20
Maximum and minimum particle radius ratio	15	Flat nodal modulus Ec/GPa	5

The 3D view of the PFC3D model of a standard uniaxial compression specimen of rock is shown in Fig. 3. The size of this numerical simulation is 50 mm × 100 mm, and finally 12,545 particles and 52,002 contacts were generated. Among the generated particles, the smallest particle size is 0.15mm, and the ratio of maximum to minimum particle size is 15.

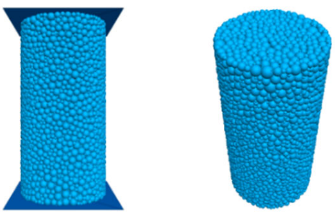

Figure 3. Standard uniaxial compression sample discrete element model

ISSN: 2710-0588

2.3. Numerical simulation programme

The defective rock samples were prefabricated by deleting the particles from the intact cylinder according to the fine-scale parameters obtained above, and the distribution of the defective rock samples was considered for the following two scenarios: (a) for the model containing a single pore and (b) for the model containing a pore-fracture.

(1) Modelling of rock samples containing a single pore: 6 different pore diameters were designed, d=0, 6, 10, 16, 20 and 26 mm. the sample with a diameter of 0 is essentially a complete cylindrical rock sample.(2) Hole-containing fissure model: In order to explore the effect of different lengths and widths of fissures on the mechanical properties of rocks, two vertical fissures with lengths of d=10mm, d=20mm, d=30mm, and widths of l=1mm, l=2mm, and l=3mm over the centre of the circle were prefabricated on the rock samples with a hole diameter of 6mm, and a total of nine kinds of fissures.

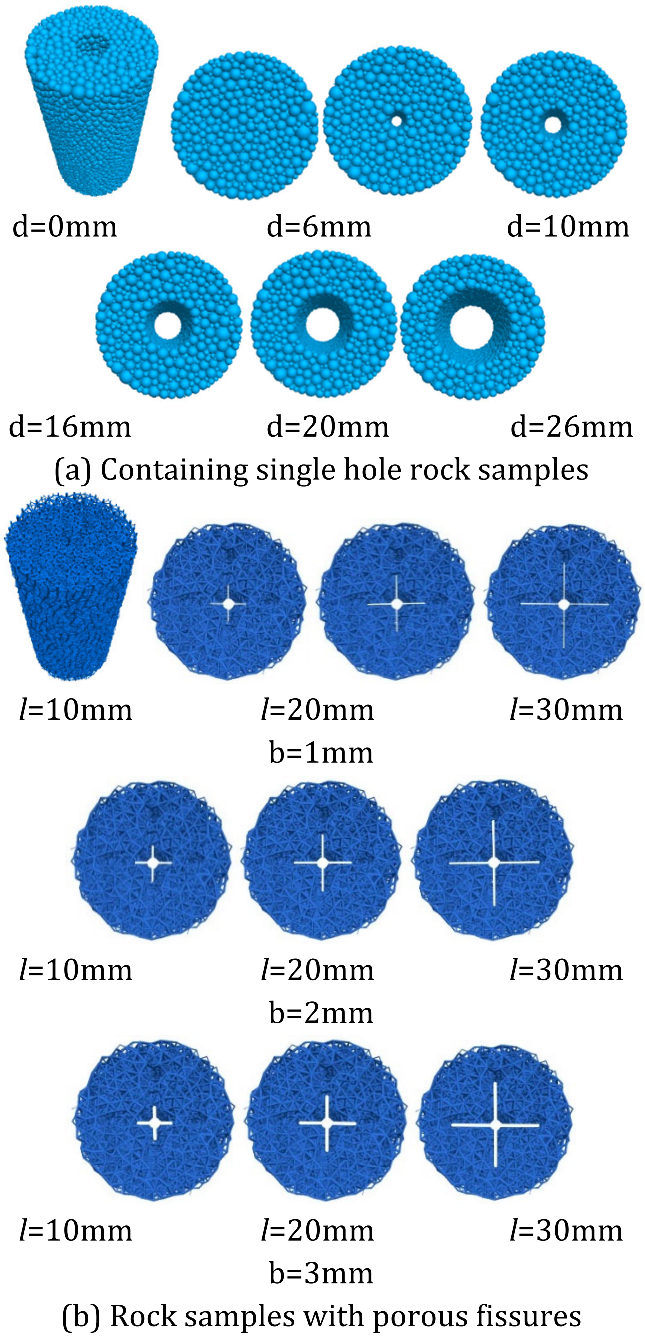

Figure 4. Sketch of deep limestone sandstone samples containing flaws

ISSN: 2710-0588

3. Mechanical Characterisation of Deep Grey Sandstone with Porous Fractures

3.1. Mechanical characterisation of deep grey sandstone with single pore hole

In order to explore the influence of different pore sizes on the mechanical properties of dark limestone such as peak strength and elastic modulus, a uniaxial compression test was carried out on rock samples with different pore sizes using PFC3D. Fig. 5 is the stress-strain curve under different pore sizes, and Fig. 6 is the peak stress and peak strain variation diagram of rock samples with different pore sizes, and the relevant specific mechanical parameters are shown in Table 2, where d=0mm rock samples represent complete rock samples.

As can be seen from Fig. 5 and Fig. 6, the uniaxial compressive strength and peak strain of the porosity rock sample are reduced compared with the intact rock sample. And the reduction is affected by the pore size. As can be seen from Table 2, the degree of decline of various mechanical parameters has a great relationship with the size of the hole. In general, the peak stress and peak strain of the deep limestone rocks containing holes decrease with the increase of pore size.

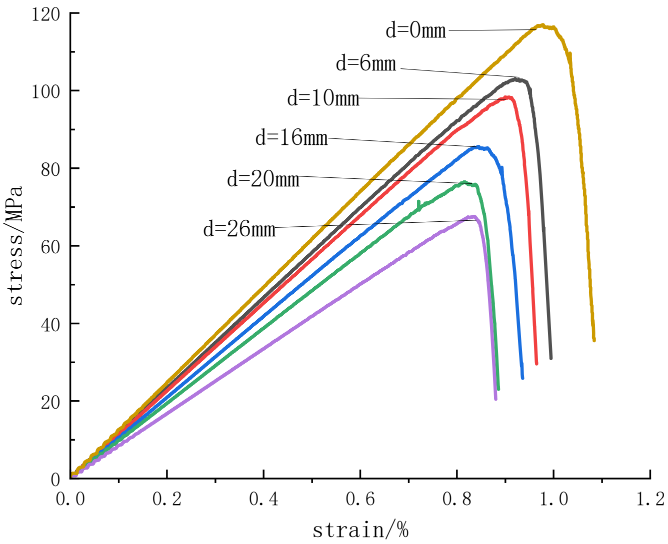

Figure 5. Stress-strain diagram

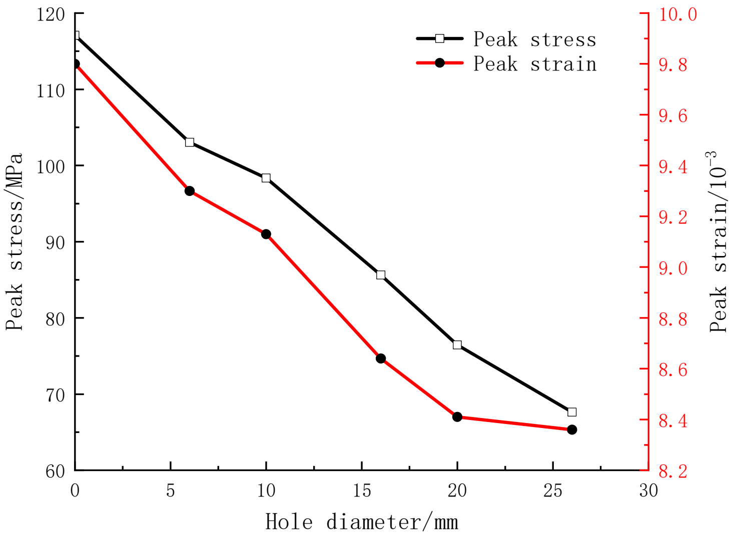

Figure 6. Peak Stress versus Peak Strain Graph

ISSN: 2710-0588

Table 2. Mechanical parameters of sandstone containing hole

Operating conditions	Peak stress /MPa	Peak strain /10^{-3}
d=0mm	117.08	9.80
d=6mm	103.03	9.30
d=10mm	98.35	9.13
d=16mm	85.63	8.64
d=20mm	76.46	8.41
d=26mm	67.64	8.36

The elastic modulus E is the slope value of the stress-strain curve in the elastic stage in rock compression, and the slope value at the peak value of the stress-strain curve at 30%~70% is taken in this paper, and the ratio of the origin of the stress-strain curve to the peak point of the stress-strain curve is taken for the deformation modulus Es, and the elastic modulus and deformation modulus of different aperture models are fitted, see Fig.

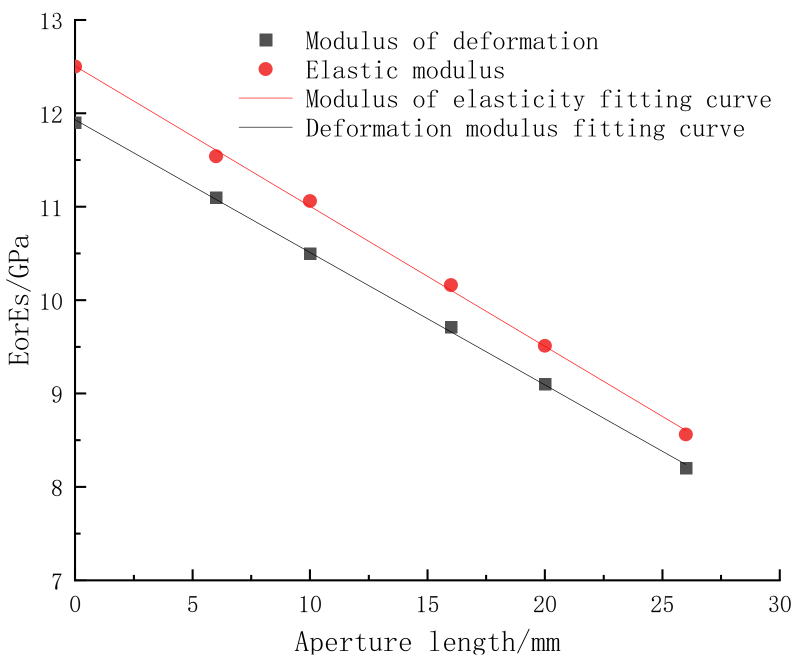

Figure 7. Fitting curves of elastic modulus and deformation modulus

It can be seen from Fig. 7 that the elastic modulus and deformation modulus of the deep limestone rock sample with a single hole are closely related to the hole diameter, and both decrease linearly with the increase of hole size.

3.2. Analysis of mechanical properties of deep limestone with pores and fissures

All fractures are prefabricated on rock samples with a hole diameter of 6mm. Fig. 8 shows the axial stress-axial strain test curves of deep limestone with cavities and fractures under uniaxial compression, and Table 3 shows the mechanical parameters of sandstone with holes and fractures. Among them, the l=0mm rock sample is the cavern rock sample with only 6mm hole diameter, and its peak stress and peak strain can be seen from Table 2 to be 103.03MPa and 9.30×10^{-3}, respectively.

ISSN: 2710-0588

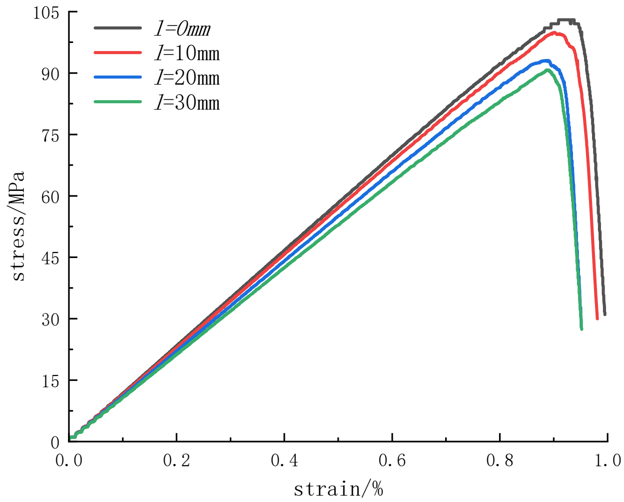

(a) b=1mm Fracture diagram

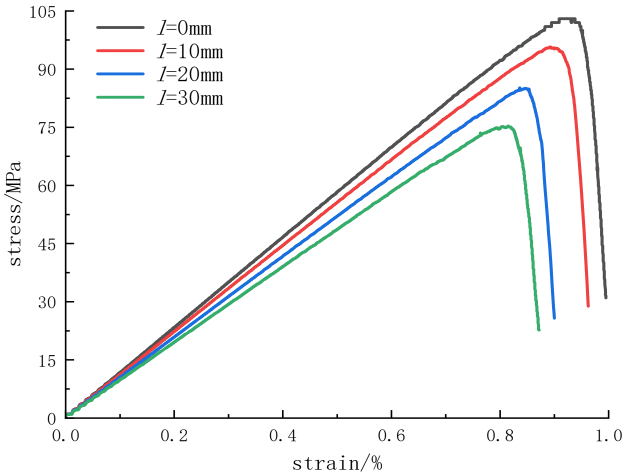

(b) b=2mm Fracture diagram

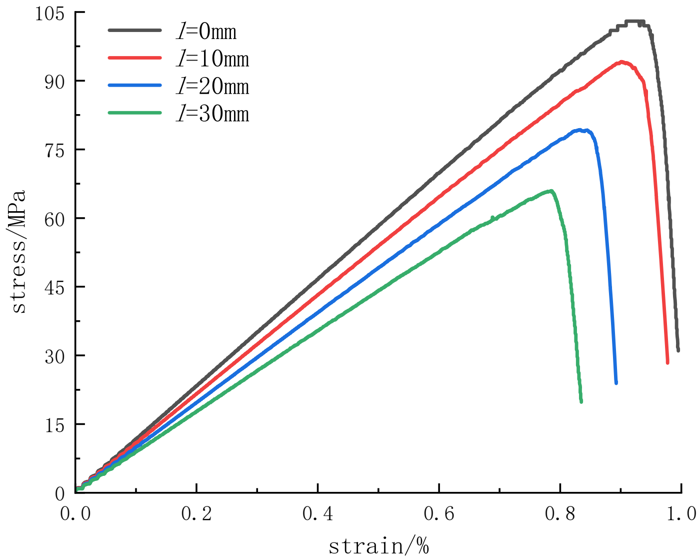

(c) b=3mm Fracture diagram

Figure 8. Axial stress-axial strain curves of deep grey sandstone containing a single hole and fissure under uniaxial compression

As can be seen from Figure 8, with the increasing width and length of fractures, the uniaxial compressive peak strength and peak strain of the rock sample are decreasing.

Comparing the constant fracture width, it can be seen from Table 3 and Table 4 that:

When the fracture width is 1mm, the uniaxial compressive strength of the rock samples with a fracture length of 10mm, 20mm and 30mm decreases to 99.92MPa, 93.10MPa and 90.70MPa, respectively, and the uniaxial compressive strength decreases by 3.02%, 9.64% and 11.97% compared with the 103.03MPa of the rock samples with only holes. The peak strain of the rock samples decreased to 9.02×10-3, 8.86×10-3 and 8.66×10-3, respectively, and the peak strain decreased by 3.01%, 4.73% and 6.88% compared with the 9.30×10-3 of the rock samples with only holes.

When the fracture width is 2mm, the uniaxial compressive strength of the rock samples with a fracture length of 10mm, 20mm and 30mm decreases to 95.77MPa, 85.05MPa and 74.47MPa, respectively, and the uniaxial compressive strength decreases by 7.04%, 17.45% and 27.72% compared with the 103.03MPa with only holes. The peak strain of the rock samples decreased to 8.93×10-3, 8.48×10-3 and 7.97×10-3, respectively, and the peak strain decreased by 3.98%, 8.82% and 14.30% compared with the 9.30×10-3 of the rock samples with only holes.

When the fracture width is 3mm, the uniaxial compressive strength of the rock sample decreases to 94.23MPa, 79.28MPa and 66.64MPa, respectively, and the strength decreases by 8.54%, 23.05% and 35.49% compared with the 103.03MPa of the rock sample with only holes. The peak strain of the rock samples decreased to 8.82×10-3, 8.45×10-3 and 7.85×10-3, respectively, and the peak strain decreased by 5.16%, 9.14% and 15.59% compared with the 9.30×10-3 with only cavities.

It can be seen that when the fracture width is constant, with the increase of fracture length, the peak strength and peak strain of the deep grey sandstone with porous fractures also show an attenuation trend. Moreover, when the fracture width increases, the peak intensity and peak strain attenuation trend of deep limestone with cavity fractures will become more and more obvious.

Table 3. Summary of peak stresses of deep grey sandstone containing hole and fissure

	Peak stress /MPa		
Operating conditions	*l*=10mm	*l* =20mm	*l* =30mm
b=1mm	99.92	93.10	90.70
b=2mm	95.77	85.05	74.47
b=3mm	94.23	79.28	66.64

Table 4. Peak strains of deep grey sandstone containing hole and fissure

	Peak strain /10^{-3}		
Operating conditions	*l* =10mm	*l* =20mm	*l* =30mm
b=1mm	9.02	8.86	8.66
b=2mm	8.93	8.48	7.97
b=3mm	8.90	8.45	7.85

4. Analysis of Microcrack Formation Process

4.1. Analysis of microscopic crack formation process in deep-limestone with single hole

Fig. 9 shows the variation process of internal microcracks in rock-like specimens under uniaxial compression when the hole diameters are 0mm, 6mm, 10mm, 16mm, 20mm, and 26mm, respectively, corresponding to the initiation stage when the crack first occurs, the expansion stage when the crack begins to generate in large quantities, and the final fracture stage when the rock sample fails, where the blue represents the microcracks caused by tensile failure, and the red represents the microcracks generated by shear failure.

As can be seen from Figure 9:

Tensile microcracks exist in the whole process from compression to complete instability of rock samples, and the crack growth rate is the largest when the loading stress is similar to the compressive strength of the sample. In the intact rock-like sample, the initial microcracks are formed on the upper and lower end faces of the sample, and there are only a few shear cracks, while there are a large number of tensile microcracks in the sample, and the tensile failure is the main one. The initial microcracks of the rock specimens with holes appear in the tensile stress concentration area perpendicular to the load direction, and no significant microcracks will appear when the load is small, and with the increase of load, the microcracks will continue

ISSN: 2710-0588

to develop along the upper and lower interfaces of the sample, and the number of shear microcracks will also increase while a large number of tensile microcracks are generated, and the final specimen will be damaged.

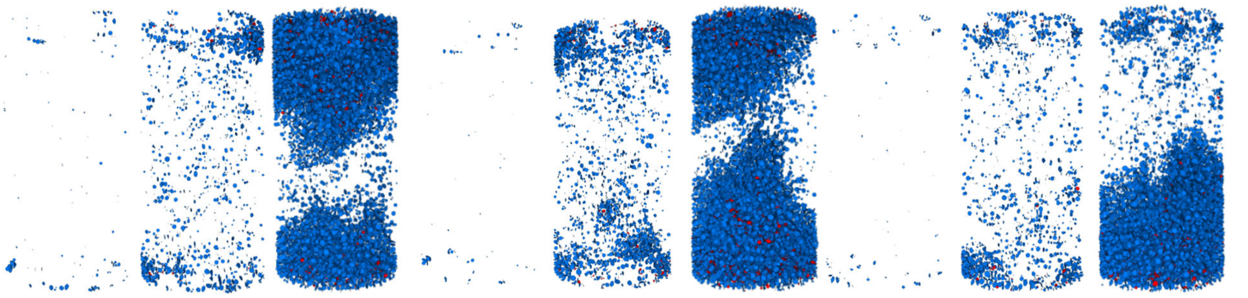

(a) The diameter of the hole is 0mm (b) The diameter of the hole is 6mm (c) The diameter of the hole is 10mm

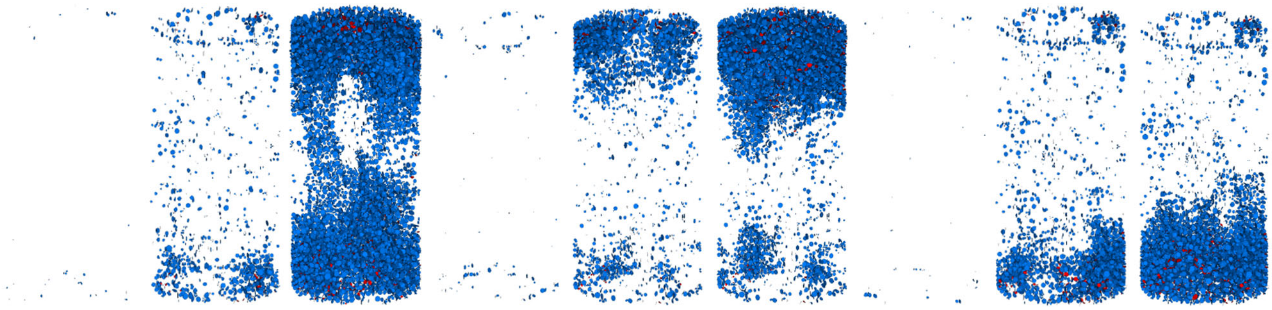

(c) The diameter of the hole is 10mm (d) The diameter of the hole is 16mm (f) The diameter of the hole is 26mm

Figure 9 Micro - cracks in rock samples with different pore diameters

Fig. 10 shows the variation curve of the number of microcracks automatically generated by PFC3D with axial strain, and it can be seen that the number of microcracks generated by rock specimens with different pore sizes increases with the increase of axial strain under uniaxial compression. The process is divided into four stages.

(1) OA in the initial compaction stage: when the specimen is in this loading stage, the original pores in the model are gradually closed due to the force, and the stress value has not yet reached the parallel bond strength between the particles, and there are almost no microcracks.

(2) Elastic stage AB: After the pores are completely compacted by stress, a small number of microcracks will be generated inside the specimen.

(3) Crack stable propagation stage BC: This stage is in the late stage of the elastic stage and the early and middle stages of the plastic stage, with the increase of strain, the microcracks increase at a slow rate, and when the loading stress is close to the peak compressive strength, the microcracks begin to expand, and the growth rate is significantly accelerated.

(4) Crack penetration stage CD: This stage is in the late stage of the plastic stage and the post-peak stage, when the peak strength is reached, with the continuous loading of stress, the specimen has a macroscopic failure surface, and the microcracks basically do not continue to occur. When the peak strength is reached, the number of microcracks produced by the rock-like specimens with aperture 0 mm and 6 mm is higher than that of the rock-like specimens with aperture of 10 mm and 16 mm, and the number of microcracks produced by the rock-like specimens with 10 mm and 16 mm aperture is greater than that of the rock-like specimens with aperture of 20 mm and 26 mm, that is, the smaller the pore size, the more microcracks are generated when the peak strength is reached.

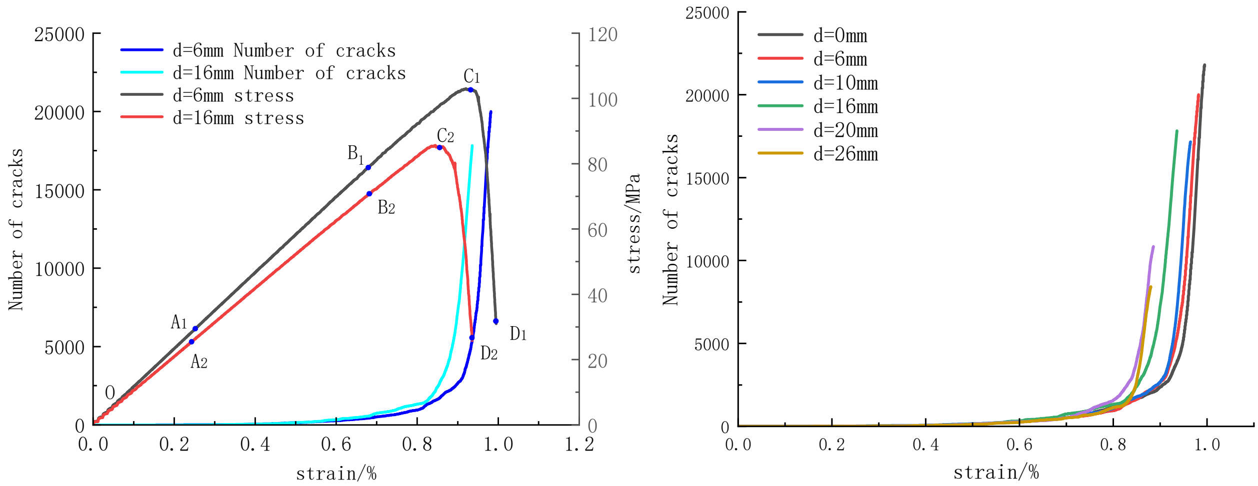

Figure 10. Variation curves of micro-cracks with axial stress- axial strain

4.2. Analysis of microscopic crack formation process in deep limestone with porous fissures

Fig. 11 shows the variation of internal microcracks in rock samples with porous fractures under uniaxial compression. Blue represents microcracks caused by tensile failure, while red represents microcracks caused by shear failure.

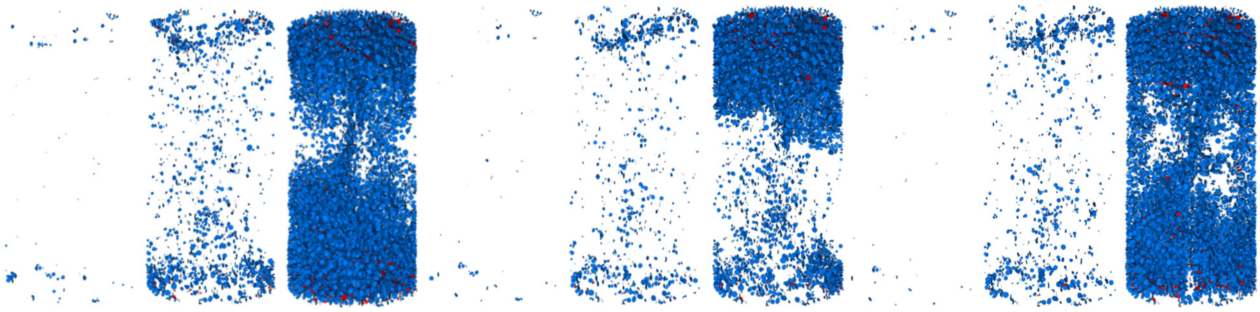

(a) The width is 1mm long is 10mm (b) The width is 1mm long is 20mm (c) The width is 1mm long is 30mm

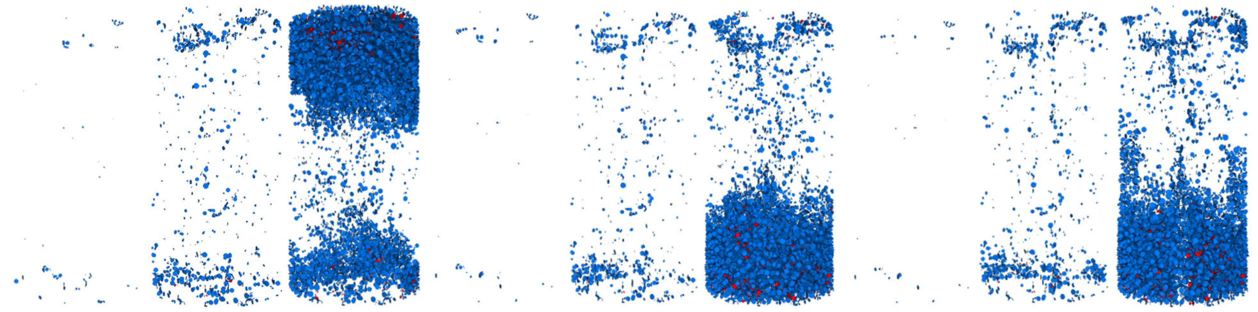

(d) The width is 2mm long is 10mm (e) The width is 2mm long is 20mm (f) The width is 2mm long is 30mm

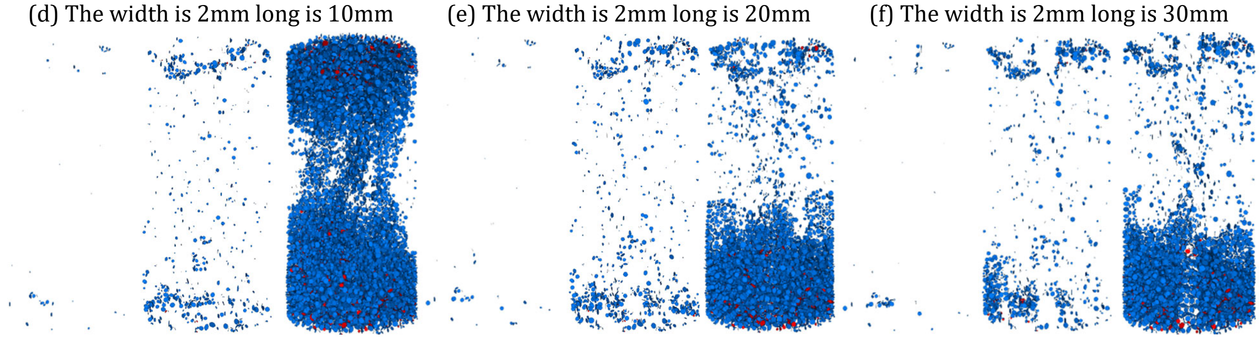

(g) The width is 3mm long is 10mm (h) The width is 3mm long is 20mm (i) The width is 3mm long is 30mm

Figure11. Micro - cracks in rock samples with different fracture

ISSN: 2710-0588

It is clear from Figure 11 that in all rock specimens, tensile microcracks are initially generated in areas of stress concentration at the upper and lower edges of the rock. Subsequently, with the gradual increase of stress, the initial tensile cracks continued to develop along the axial direction, with a small number of microcracks in the middle, a large number of tensile microcracks and a small number of shear microcracks at both ends, and finally the tensile cracks were mainly concentrated at both ends of the rock sample, and the specimen was damaged, and the failure mode was about the same as that of the rock sample with holes.

Fig. 12 is a graph of the number of microcracks in different fractured rock samples, from which it can be seen that the formation of microcracks is almost negligible in the initial compression stage of the sample. In the second half of the elastic phase BC, microcracks begin to appear and gradually increase with increasing deformation. When the applied stress is close to the peak compressive strength, the diffusion and growth rate of microcracks rise dramatically.

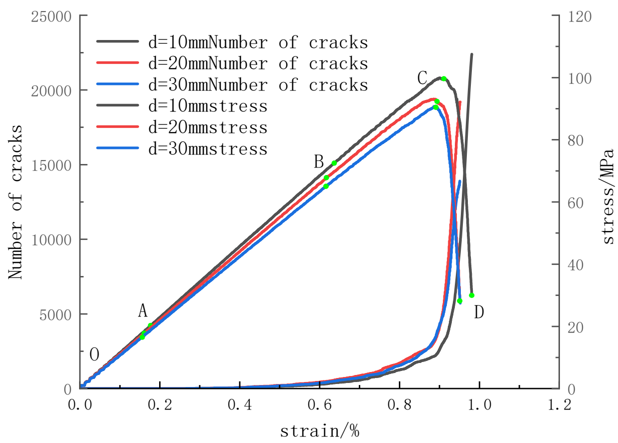

(a) The width of the fissure is 1mm

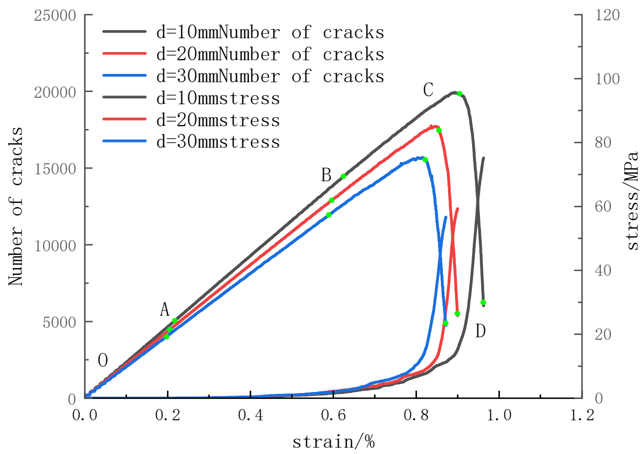

(b) The width of the fissure is 2mm

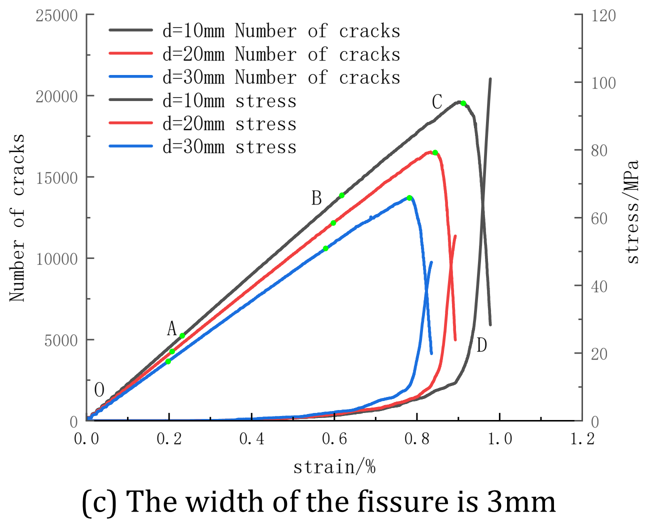

(c) The width of the fissure is 3mm

Figure 12. Variation curves of micro - cracks with axial strain

The test results show that the width and length of the fracture have a significant effect on the number of microcracks, and the rock samples with shorter fracture length will produce more microcracks when the peak strength is reached when the fracture width is constant. Similarly, in the case of a fixed fracture length, the smaller the fracture width, the greater the number of microcracks at peak strength.

ISSN: 2710-0588

5. Mechanism of Energy Evolution

5.1. Principles of energy calculation

Assuming that there is no heat exchange with the outside world during this uniaxial compression test, U is the work done by the external force on the rock, that is, the energy absorbed by the rock. From the law of conservation of energy, it can be seen that

$$U=Ue+Ud \tag{1}$$

where: U_e is the elastic strain energy stored in the rock; U_d is the energy dissipated by the rock during the loading process, which is mainly used for internal damage and plastic deformation of the rock. The correspondence between the dissipated energy Ud and the elastic strain energy U_e is shown in Figure 13

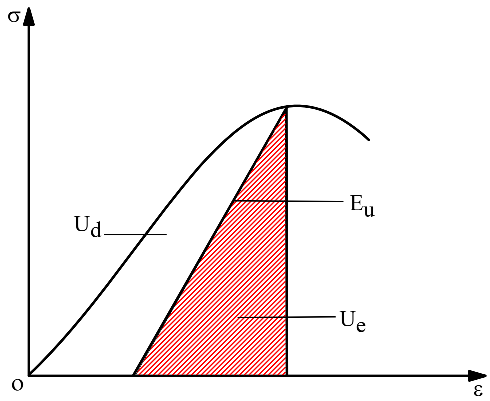

Figure 13. Diagram of dissipative energy and elastic strain energy

The shaded part of Fig. 11 is the elastic strain energy U_e, and the part enclosed by the unloading modulus Eu, the stress-strain curve, and the transverse axis is the dissipated energy U_d.

In the triaxial state, the energy calculation of the rock mass can be expressed as:

$$U=\int_0^{\varepsilon_1}\sigma_1\,d\varepsilon_1+\int_0^{\varepsilon_2}\sigma_2\,d\varepsilon_2+\int_0^{\varepsilon_3}\sigma_3\,d\varepsilon_3 \tag{2}$$

$$U_e=\frac{1}{2}\sigma_1\varepsilon_{e1}+\frac{1}{2}\sigma_2\varepsilon_{e2}+\frac{1}{2}\sigma_3\varepsilon_{e3} \tag{3}$$

$$\varepsilon_{ei}=\frac{1}{E_u}\left[\sigma_i-v_u\left(\sigma_j+\sigma_k\right)\right] \tag{4}$$

Eq. (3) can be rewritten as:

$$U_e=\frac{1}{2E_0}\left[\sigma_1^2+\sigma_2^2+\sigma_3^2-2v(\sigma_1\sigma_2+\sigma_2\sigma_3+\sigma_3\sigma_1)\right] \tag{5}$$

where σ_i is the principal stress, ε_i is the principal strain, ε_{ei} is the corresponding elastic strain, E0 and Eu are the initial modulus and unloading modulus, respectively, and vu is the Poisson's ratio.

This test is a uniaxial compression test, so the second and third principal stresses are 0, and in this test, Eu and E0 can be approximate replaced, and the energy calculation expression is:

ISSN: 2710-0588

$$U = \int_0^{\varepsilon_1} \sigma_1 \, d\varepsilon_1 \tag{6}$$

$$U_e = \frac{1}{2E_u}\sigma_1^2 \tag{7}$$

$$U_d = U - U_e \tag{8}$$

5.2. Energy evolution analysis of deep limestone with holes

Fig. 14 shows the energy conversion diagram of dark limestone with different pore sizes for uniaxial compression test:

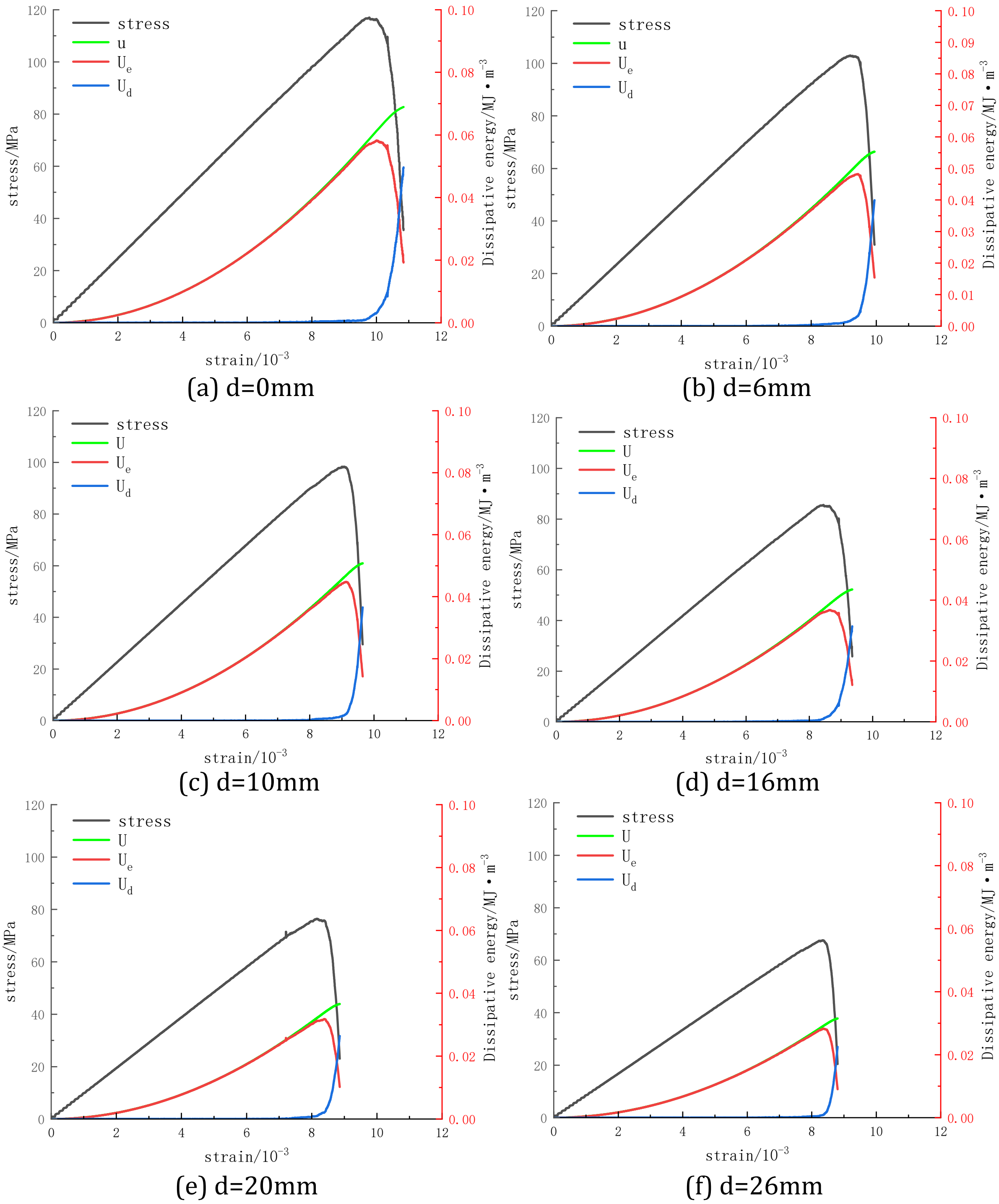

Figure 14. Diagram of dissipative energy and elastic strain energy

Analysis of Figure 14 yields the following pattern:

(1) Elastic stage: In this stage, it can be seen that the total energy U and the elastic strain energy U_e curve are about the same, and in this stage, almost all of them become elastic deformation energy due to the action of external force, and there is almost no damage to the rock mass.

(2) Yield stage: At this stage, the total energy U is still basically converted into elastic strain energy U_e, and then with the gradual increase of external force, damage begins to appear in the rock mass, and the dissipated energy U_d begins to increase gradually.

(3) Post-peak stage: In this stage, the total energy U throw continues to increase, the elastic strain energy U_e in the rock mass begins to decrease sharply, the dissipated energy U_d begins to increase sharply, the rock is damaged, and the dissipated energy is used for the consumption of rock failure.

By observing the curve variation law of Fig. 14, it can be found that with the continuous increase of rock aperture, the strain node of dissipated energy begins to appear earlier, from 0.0088 of intact rock to 0.0081 of 26mm, indicating that the damage inside the rock will become more and more serious when the rock aperture is larger.

In order to understand the relationship between the hole diameter and the rock energy storage limit more intuitively, the change fitting diagram of the energy storage limit and the hole size is drawn, as shown in Figure 15.

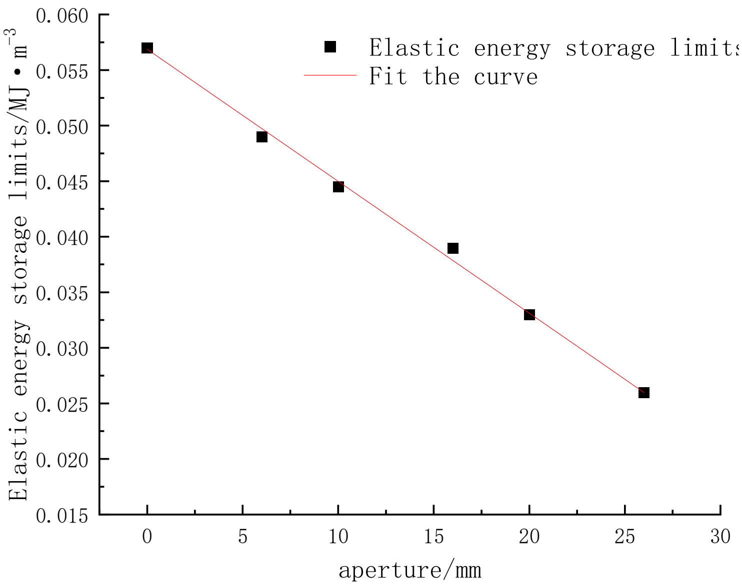

Figure 15. Relationship between different apertures and elastic energy storage limits

As we can see from the figure, the elastic energy storage limit of the rock gradually decreases as the pore size increases. When the rock is a complete rock sample, the rock strength is the largest, and the latest failure occurs, and with the continuous increase of the rock aperture, the rock strength gradually decreases, that is, when the pore diameter is 26mm, the earliest failure occurs.

6. Conclusion

(1) The mechanical parameters of the deep-lime sandstone sample with holes are obviously lower than those of the normal rock sample, and the decrease of the mechanical parameters is closely related to the diameter of the hole, with the increase of the diameter of the hole, the peak stress, peak strain and elastic modulus of the deep-lime sandstone sample with holes

ISSN: 2710-0588

show an attenuation trend, while the different defect states of the rock sample with holes and fractures will also lead to the weakening of the mechanical parameters of the deep-lime sandstone.

(2) The microcracks generated by the deep limestone sandstone samples with holes and hole-bearing fractures are mainly distributed at both ends of the rock samples, and there are fewer microcracks in the middle area, and the main microcracks are tensile microcracks, and a small number of shear microcracks are produced at the end. The results show that the tensile failure is mainly due to the action of uniaxial compression, and the number of microcracks is closely related to the hole cracks, and the number of microcracks shows an attenuation trend with the increase of hole diameter, fracture length and width.

(3) The pore size of the rock has a great influence on the energy storage limit, with the increase of the pore size of the rock sample, the strain node where the dissipated energy begins to appear gradually becomes earlier, the energy storage capacity of the rock is greatly reduced, and the internal damage becomes more and more serious.

Acknowledgements

Supported by the National Natural Science Foundation of China under Grant No. U1604142: Henan Province Key R&D and Promotion Special Project (212102310405)

References

[1] Li D Y, LIU M, HAN Z Y .et al. Experimental study on dynamic compressive mechanical properties of pore-bearing laminated sandstone[J]. Journal of Coal,2019, 44(05):1349-1358.

[2] YANG S Q, LU Z H, QU T. Detailed experiments and simulation of crack extension in marble with single pore[J]. Journal of China University of Mining and Technology,2009, 38(6):774-781.

[3] Li X H, NIU Z J, YAO Q L. et al. Particle flow analysis of fracture extension characteristics in porous trident-fractured sandstone[J]. Journal of Coal,2020, 45(11):3735-3747.

[4] FU M Z, SUN X. Analysis of the influence of the distribution of pore-fracture combinations on the mechanical properties of rocks based on discrete elements[J]. Guangdong Building Materials,2023, 39(12):62-65.

[5] DUAN J C, TANG C A, CHANG X. et al. Mechanical behaviour of porous brittle materials under uniaxial compression[J]. Geotechnics,2006, (08):1416-1420.

[6] HAN G S, JING H W, SU H J. et al. Strength and deformation damage characteristics of sandstone with prefabricated double circular holes[J]. Journal of Coal,2017, 42(04):871-878.

[7] ZHANG Q W, GAO B. B., MA L J. et al. Research on the crack evolution law of sandstone containing double holes[J]. Journal of Underground Space and Engineering,2016, 12(S2):432-437.

[8] ZHU T T, JING H W, SU H J. et al. Experimental study on uniaxial compressive mechanical properties of sandstone containing double circular holes[J]. Journal of Geotechnical Engineering,2015, 37(06):1047-1056.

[9] XIE L M, ZHU W C, WANG S H. et al. Parallel computational analysis of three-dimensional rupture process in rock specimens with holes[J]. Journal of Geotechnical Engineering,2011, 33(09):1447-1455.

[10] Zhang X P ,Wong L.Cracking Processes in Rock-Like Material Containing a Single Flaw Under Uniaxial Compression: A Numerical Study Based on Parallel Bonded-Particle Model Approach[J].Rock Mechanics & Rock Engineering, 2012, 45(5):711-737.

[11] Gong S, Zhao Y X, Zhou L, et al. Dynamic fracture behaviour of limestone with double pore cracks under impact loading[J]. Journal of Coal Science,2023,48(08):3030-3047.

[12] Wang Y ,Xu M ,Kong D , et al. Study on destabilization failure characteristics and energy evolution law of drilling holes [J]. Energy Science & Engineering, 2023, 11 (8):2818-2830.

ISSN: 2710-0588

[13] LI Y H, LIU J S, TANG X J. et al. Simulation analysis of mechanical properties of porous soft rock body considering fracture[J]. Journal of Mining and Safety Engineering, 2020, 37 (03):594-603.

[14] HUANG S L, ZHONG P J, DING X L. Anisotropic characterisation of uniaxial compressive characteristic strength of chlorite schist [J]. Journal of Rock Mechanics and Engineering, 2021, 40 (S2):3182-3190.

[15] Fan X ,Jiang X X ,Liu Y X. Local stress distribution and evolution surrounding flaw and opening within rock block under uniaxial compression [J]. Theoretical and Applied Fracture Mechanics, 2021, 112.

[16] Li X J ,Bai Y F ,Chen X D. Experimental and numerical study on crack propagation and coalescence in rock-like materials under compression [J]. The Journal of Strain Analysis for Engineering Design, 2021, 56 (8):548-562.

[17] DU M R, JING H W, SU H J.Research on the effect of elliptical holes on strength and deformation characteristics of sandstone specimens[J]. Journal of Mining and Safety Engineering,2017, 34(01):141-147.

[18] ZHANG C, TANG J X, TENG J Y. et al. Experimental study on the effect of the number of holes and pore diameter on the mechanical properties of marble[J]. Geotechnics,2017, 38(S2):41-50.

[19] WANG Y F, ZHENG X J, JIAO H Z et al. Energy evolution mechanism and energy yielding criterion of granite damage process[J]. Explosion and Impact,2016, 36(06):876-882.

[20] WANG Y F, HUANG Z J, CUI F. Fine-scale mechanical damage evolution mechanism of coal rock damage process[J]. Journal of Coal,2014, 39(12):2390-2396.

[21] CHENG H M, YANG X B, YANG D H et al. Characteristics of energy conversion and inclination effect in fractured sandstone under uniaxial compression[J]. Coal Engineering,2023, 55(10):143-148.

[22] YU Y, WANG Z H, TANG C X. Energy evolution and fractal characteristics of acid-eroded granite under uniaxial compression[J]. Geotechnics,2023, 44(07):1971-1982.